# Computation of damped nonlinear normal modes for large scale nonlinear systems in a self-adaptive modal subspace

Jie Yuan[a,b,*], Yekai Sun[a], Christoph Schwingshackl[a], Loic Salles[a]

[a] *Vibration University Technology Centre, Imperial College London SW7 2AZ, London,UK*
[b] *Aerospace Centre of Excellence, University of Strathclyde, Glasgow, G1 1XQ, UK*

**Abstract**

The concept of nonlinear modes has been proved useful to interpret a wide class of nonlinear phenomena in mechanical systems such as energy dependent vibrations and internal resonance. Although this concept was successfully applied to some small scale structures, the computational cost for large-scale nonlinear models remains an important issue that prevents the wider spread of this nonlinear analysis tool in industry. To address this challenge, in this paper, we describe an advanced adaptive reduced order modelling (ROM) technique to compute the damped nonlinear modes for a large scale nonlinear system with frictional interfaces. The principle of this new ROM technique is that it enables the nonlinear modes to be computed in a reduced self-adaptive modal subspace while maintaining similar accuracy to classical reduction techniques. The size of such self-adaptive subspace is only proportional to the number of active slipping nodes in friction interfaces leading to a significant reduction of computing time especially when the friction interface is in a micro-slip motion. The procedure of implementing this adaptive ROM into the computation of steady state damped nonlinear mode is presented. The case of an industrial-scale fan blade system with dovetail joints in aero-engines is studied. Damped nonlinear normal modes based on the concept of extended periodic motion is successfully calculated using the proposed adaptive ROM technique. A comparison between adaptive ROM with the classical Craig-Bampton method highlights the capability of the adaptive ROM to accurately capture the resonant frequency and modal damping ratio while achieving a speedup up to 120. The obtained nonlinear modes from adaptive ROM are also validated by comparing its synthesized forced response against the directly computed ones using Craig-Bampton (CB) method. The study further shows the reconstructed forced frequency response from damped nonlinear modes are able to accurately capture reference forced response over a wide range of excitation levels with the maximum error less than 1% at nearly zero computational cost.

*Keywords:* Damped nonlinear modes, Adaptive reduced order modelling, Joint Structures, Harmonic balanced methods

*Corresponding author
*Email address:* jie.yuan@strath.ac.uk (Jie Yuan)

## 1. Introduction

Nonlinearity is widely existing in engineering structures in many different forms such as friction in bolted joints, large amplitude vibrations, material behaviour, or fluid-structure interactions [1, 2, 3]. These nonlinearties can pose a big challenge to engineers because nonlinear systems can exhibit a wide range of complex dynamic characteristics that are very difficult to predict and potentially catastrophic. Therefore, the dynamic analysis of structures with nonlinear characteristics is becoming an important topic in different engineering fields to drive an improved design to ensure high structural efficiency and reliability. Those nonlinearities involved in a complicated engineering system can be broadly classified into two main types, which are distributed and localised nonlinearities. Geometrical nonlinearity is mainly due to large amplitude vibrations. It is a typical example of distributed nonlinearities where the nonlinearities is distributed among all degrees of freedom in a whole structure. In terms of localised nonlinearities, the contact friction is one of typical examples, which are widely existing in large scale assemblies particularly in a jet engine. Such a localised nonlinearity in a large scale engineering system is the focus of this study. The main feature of such a system is that, depending on the level of motion, very different levels of energy dissipation can be achieve through the friction interfaces ranging from full stuck to fully sliding contact. Such a dissipation from the nonlinear contact friction force also leads to a reduction in the global stiffness of the system and generate a strong energy dependent damping, resonant frequency and also instability problems [4, 5, 6, 7, 8]. These inherent nonlinearities are however often ignored or linearised or simplified for the design of a large scale system due to high computational expense and numerical instability problems [9]. To ensure an improved design of such nonlinear systems, effects of localised nonlinearities on the dynamics must be taken into account through an efficient nonlinear analysis tool [10].

Nonlinear modal analysis becomes an increasingly popular tool to give an insight into the response of a nonlinear system [1, 2, 3]. The concept of nonlinear modes is to extend the modal analysis of a linear system. In a linear system, the free vibration response is defined as the linear normal mode. As an extension of linear normal mode in nonlinear system, nonlinear mode can be considered as limit cycle oscillation, but also are general solutions of an autonomous system. This concept has been proved very useful to interpret a wide class of nonlinear phenomena such as energy dependent damping and resonance, mode localisation, internal resonance and the stability of the system [3]. Compared with linear normal mode, the superposition principle and orthogonality between different modal deflection shapes are not valid for nonlinear system. Also, it would not guarantee the uniqueness of the solutions and some of these solutions might be unstable. However, similar to linear modes, the nonlinear modes can still reproduce the resonant vibration behavior subjected to harmonic excitation. Furthermore, the invariance property in the resonant response also applies to nonlinear mode. The foundation of theory of nonlinear mode can be traced back to centre theorem from Lyapunov and Poincaré [11, 12]. The first definition of nonlinear normal modes (NNM) was given by Rosenberg [13] who defined NNM for a conservative system as periodic unison motion where all points in a system reach their equilibrium position and their extreme position simultaneously. However, this definition

of NNM cannot be used to explain internal resonances. Shaw and Pierre then defined the NNM as an invariant manifold in phase space which is tangent to the eigenspace of the linear modes at the equilibrium points [14]. This definition allows the concept of NNM to capture the internal resonance and be extended to a non-conservative system that include damping terms. This type of NNM was defined as damped Nonlinear Normal Mode (dNNM). Since then, NNM computation was further extended to nonlinear systems with strong dissipation by Laxalde and Krack [15, 16]. Laxalde extended the concept of complex linear modes to nonlinear and non-conservative systems based on a definition of eigenfunctions as generalized Fourier series. Thanks to the definition of this complex nonlinear modes, the computation of dNNMs for a large scale structure with friction interface is achievable. Krack further developed a numerical method, namely Extended Periodic Motion Concept (EPMC), to compute a dNNM based on a enforced periodic concept by introducing an artificial damping term to balance the dissipated energy from the non-conservative nonlinear force [17]. Compared to the method presented in [18], EPMC has shown a better quantification of energy dissipation within the system and works well when the system is highly damped [19]. The EPMC is therefore used in this study for the computation of dNNMs for a large scale system with contact friction nonlinearties.

Another main benefit of dNNMs is that forced frequency response can be synthesised from obtained dNNMs without large computational efforts. One of main techniques for nonlinear modal synthesis is based on single nonlinear resonant mode theory [20]. It assumes that a single nonlinear mode dominates the system response and is treated as nonlinear while the remaining modes are approximated by their linearised counterpart because of their low energy levels. Krack has applied this method to the system with contact friction [21]. Grolet and Sarrouy also employed this method to reconstruct the forced response of a geometrically nonlinear system using a amplitude-phase formulation [22, 23, 24]. The study by Sarrouy found that the forced response synthesised from dNNMs can achieve a better accuracy than undamped NNMs. It was also clear that one of the main limitations about this nonlinear modal synthesis is that it is not able to capture nonlinear modal interaction. The other main method to interpret forced response from NNMs is called energy balanced method (EBM). It has been attempted by Kuether and Hill [2, 25] who used it to identify the isolas and also relate the NNM to resonant solution in forced response for a conservative nonlinear system. Recently, EBM has been further extended to systems with non-conservative nonlinear system by Sun et al. [26], which is named extended energy balance method (E-EBM). The resonant response can be accurately predicted for a system with strong contact friction nonlinearties. It proves that the use E-EBM can significantly improve the efficiency and reduce the computational cost for the computation of resonant solution in a forced response, especially for structure with frictional contact. However, the effectiveness of both methods has not been compared in open literature. In this paper, the forced response interpretation from dNNMs will be demonstrated with both nonlinear modal synthesis and energy balance method.

Although dNNMs have attractive features to interpret nonlinear systems, the computation of dNNMs for a large scale system is still challenging even for the system with localised nonlinearities such as contact friction [27]. To overcome this problem, sub-structuring techniques are often used for model order reduc-

tion [10, 9, 6, 28, 29]. The main idea is to consider the components in an assembly as distinct sub-structural elements. The reduced basis for such an assembly can be then constructed with the linear normal modes and the static modes associated to the retained interface nodes from the sub-structural elements [30, 31, 32]. The reduction can effectively eliminate most internal DOFs for each component while retain the whole nonlinear DOFs [33]. The other benefit of sub-structuring methods is that it is convenient to integrate non-linear constitutive model such as friction models on the interface. However, the size of substructuring based ROMs is proportional to the size of contact interfaces. Despite of the advance in computational power, the computation of such a ROM is still very challenging for a large scale system e.g. bladed disc assembly in turbomachinery [9, 34].

To overcome above-mentioned challenges, improved sub-structuring methods are needed to enhance the computational performance for the calculation of dNNMs. Recently, an adaptive component mode synthesis method was put forward by Yuan providing a significant computational improvement for large scale systems with friction joints [35, 36, 37]. The method allows the set of static modes in classical CMS reduced basis to update automatically according to the real-time contact conditions on the interface. It was achieved by a rewritten equation of motion by combining the underling linearised system with a new adaptive internal variable that accounts the non-linear effects from contact interface. This enables the following ROM to remove a number of redundant static modes associated to sticking nodes in a self-adaptive way. Such an adaptivity can lead to a considerably computational saving for the jointed structures with micro-slip motions. This adaptive ROM can be conveniently integrated with the harmonic balance method (HBM) to obtain the most interesting steady-state response. The original adaptive algorithm was further improved by introducing an energy-based error estimator [37]. It can be effectively used as a monitoring indicator to update the set of reduced basis through adding or removing associated static modes during the online computation. The error estimator can help further increase the computational efficiency and improve the computational accuracy by eliminating numerical noise. It provides a very promising and appealing approach for the computation of dNNMs as well, which however has not been investigated yet.

This study aims to address above-mentioned industrial computational challenge on the calculation of nonlinear modes for a large scale nonlinear system. The main contribution of this work is that the adaptive ROM is introduced in the calculation of dNNMs for a large scale nonlinear system. The computing performance between adaptive ROM and the classical sub-structuring methods are compared with an industrial scale model. Furthermore, the use of nonlinear modal synthesis and energy balance method to interpret the forced response is also demonstrated and compared. The paper is organized as follows: at first, the formulation of the nonlinear mechanical system and adaptive reduced order model is presented; it is followed by the introduction of damped nonlinar modal analysis and related computational techniques to interpret the forced response; then, the implementation of adaptive ROM for the computation of dNNMs is described; after that, an industrial-scale test case, namely, fan blade system with a dovetail joint in a jet engine, is described; in the results section, the characteristic of dNNMs is firstly presented; it is then followed by a de-

tailed presentation of accuracy and speedup of using adaptive ROM compared to the classical CB method; the forced response prediction from dNNMs is finally predicted and validated by comparing against the directly computed FRFs.

## 2. Mechanical system

### *2.1. Equation of Motion*

For a mechanical system with friction interface, the equation of motion in a forced response is given as:

$$\mathbf{M}\,\ddot{u}(t) + \mathbf{C}\,\dot{u}(t) + \mathbf{K}\,u(t) + \mathrm{F}_{nl}(u(t)) = \mathrm{F}_e(\gamma, \varphi, \Omega, t) \tag{1}$$

where $\mathbf{M}$, $\mathbf{K}$ and $\mathbf{C}$ are mass matrix, stiffness matrix and viscous damping matrix respectively. $u(t)$ is the physical displacement of the structure. $\mathrm{F}_e$ is the external periodical force. $\mathrm{F}_{nl}$ is the nonlinear force involved in the system. $\Omega$ is the excitation frequency; $\gamma$ is the excitation forcing level; $\varphi$ is the absolute phase of the excitation force. For an autonomous system, the external excitation force $\mathrm{F}_e$ in Eqn.1 would be set zero. The damped nonlinear mode is considered as the solution of such an autonomous system.

## 3. Adaptive reduced order model

In this section, the contact model to predict friction force and the development of adaptive reduced order model from the original system in Eqn.1 are described.

### *3.1. Contact Model*

A 3D node-to-node contact model is used to simulate the friction force on the contact interface. As shown in Fig.1a, this model contains two coupled 1D Jenkens elements in the tangential direction with a spring in the normal direction. Two coupled tangential Jenkins elements are used to model a two dimensional in-plane motion while a coupling normal spring is used to define the contact status. Normal contact conditions are defined as two states, namely in-contact condition, and separation. If the predicted normal force $F_N$ becomes negative, separation occurs between the two contact nodes and the normal contact force becomes zero. Whereas if $F_N$ is positive, the contact pair is in contact and thus there are two types of tangential contact states possible: (i) the sticking condition which will occur when the overall tangential contact force $F_T$ is less than the Coulomb friction limit $\mu F_N$; (ii) the slipping condition which happens when the tangential contact force $F_T$ is equal or above the Coulomb friction limit $\mu F_N$. As a result, there are three general contact conditions: separation, stick and slip for each 3D node pair that can occur at any point during a vibration cycle. As shown in Fig.1a, the $k_n$ and $k_t$ are normal and tangential contact stiffness ($N/mm^3$), which is is actually the slope of the deformation at the sticking condition shown in hysteresis loop in Fig. 1b;$\mu$ is friction coefficient; $x(t)$, $y(t)$ and $z(t)$ are tangential and normal displacement in local coordinate system. The initial contact condition is defined by the pre-defined normal load $N_0$ and gap. The local contact

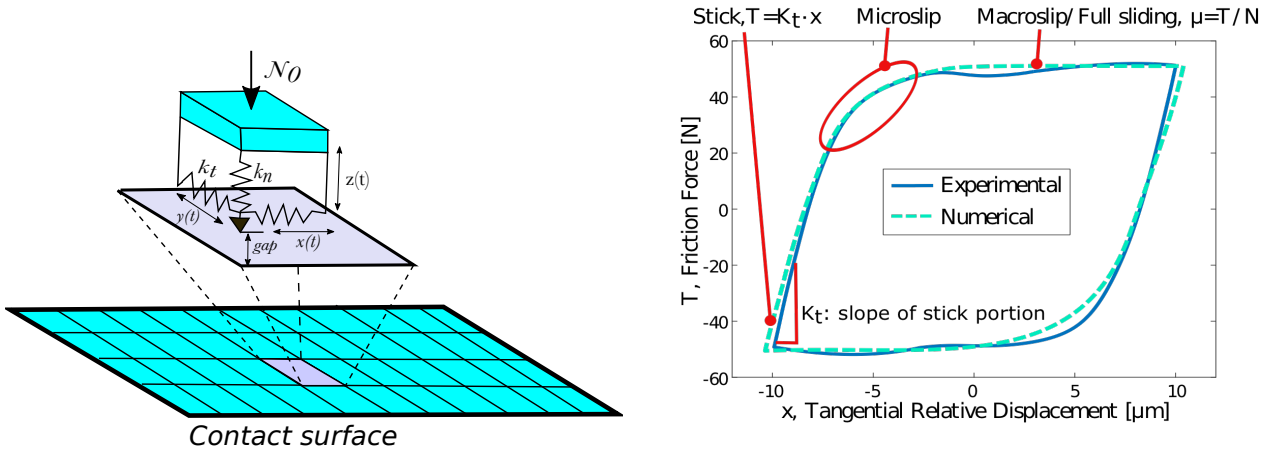


(a) (b)

Figure 1: (a) 3D node to node element (b) Hysteresis loop [41]

stiffness for each contact element is computed from the normalised contact stiffness with a unit of $N/mm^3$, obtained by measurements [38] times the area of that contact element while the global contact stiffness is the contact stiffness times the whole contact area. It is worth noting that the distribution of $N_0$ on the contact surface should be pre-identified from the experimental measurement or nonlinear static analysis as it has a large influence on the nonlinear dynamics of jointed structures. Contact stiffness should be dependent on the normal pressure. However, such a dependency is not considered in this paper due to insufficient experimental data. The interested readers can also find the detailed formulation of this contact element in [39, 40].

Figure. 1b shows a typical experimental hysteresis loop in blue, which is identified from a 1D friction test rig [38]. The tangential contact stiffness is determined experimentally by the slope of the sticking portion. The friction coefficient is identified by the ratio of tangential force to the normal load in the macroslip region. The numerical hysteresis loop obtained from a full mesh grid of 3D node-to-node contact elements shown in dashed green is compared with the experiment loop. It is found that the microslip effect observed in the experimentally measured loops, which occurs when a part of the interface is in sliding condition while the rest is in sticking, can be also captured through a combination of contact elements in the dense spatial discretization of the contact interface. This confirms that 3D contact elements are effective to represent the contact friction behaviour including the sticking, macroslip and microslip.

### *3.2. Linearised system*

To apply the adaptive ROM method, the mechanical system shown in Eqn.1 is firstly linearised on the friction interface using the contact stiffness $k_t$ and $k_n$. If the whole contact surface is in a sticking condition, the tangential and normal contact forces are equal to the linearised contact forces. However, if there is any contact pair in a slipping condition, the linearisation would not be accurate as there will be

a remainder between the linearised contact force and nonlinear contact force induced by the slipping or sepration. Therefore, an internal variable $\Delta p$ is introduced into the linearised system in order to take into account the nonlinearities from the friction interface. The internal variable $\Delta p$ for $i^{th}$ contact pair can be formulated as:

$$\Delta p^i = \begin{cases} (\mathrm{F}_T^i - k_t \Delta u_i^T)/k_t & \text{Tangential direction} \\ (\mathrm{F}_N^i - k_n \Delta u_i^N)/k_n & \text{Normal direction} \end{cases} \tag{2}$$

where $\mathrm{F}_T^i, \mathrm{F}_N^i$ is the tangential and normal force at $i^{th}$ contact node, which are evaluated for each contact pair using the 3D contact element; $\Delta u_i^T, \Delta u_i^N$ are the relative displacement at $i^{th}$ contact node. The size of $\Delta p$ is only half number of interface DOFs as the amplitudes of nonlinear force are same on both contact interfaces while only the sign is opposite. The Newton's third law is therefore implicitly taken into account in the following rewritten equation of motion. The rewritten equation of motion for adaptive ROM can be expressed as [36]:

$$\underbrace{\begin{bmatrix} \mathbf{M} & \mathbf{0} \\ \mathbf{0} & \mathbf{0} \end{bmatrix}}_{\mathbf{M^G}} \begin{bmatrix} \ddot{u} \\ \Delta\ddot{p} \end{bmatrix} + \underbrace{\begin{bmatrix} \mathbf{C} & \mathbf{0} \\ \mathbf{0} & \mathbf{0} \end{bmatrix}}_{\mathbf{C^G}} \begin{bmatrix} \dot{u} \\ \Delta\dot{p} \end{bmatrix} + \underbrace{\begin{bmatrix} \mathbf{K}_L(k_t, k_n) & \mathbf{BK_J} \\ (\mathbf{BK_J})^T & \mathbf{K_J} \end{bmatrix}}_{\mathbf{K^G}} \begin{bmatrix} u \\ \Delta p \end{bmatrix} = \underbrace{\begin{bmatrix} 0 \\ \mathrm{F}_{nl}(u) \end{bmatrix}}_{\mathbf{F_{nl}^G}} + \underbrace{\begin{bmatrix} \mathrm{F}_e \\ 0 \end{bmatrix}}_{\mathbf{F_e^G}} \tag{3}$$

where the $\mathbf{K}_L(k_t, k_n)$ is the global linearised stiffness matrix on the contact interface, which is as a function of local contact stiffnesses, $k_t, k_n$. The latter are the local tangential and normal contact stiffness of each contact element as described in the previous section; $\mathbf{K_J}$ is the linear joint stiffness matrix associated to the contact interface DOFs; $\mathbf{B}$ is the signed Boolean matrix to transform the joint matrix into the global system matrix; $\mathbf{K^G}, \mathbf{C^G}, \mathbf{M^G}$ are the linear stiffness, damping and mass matrix of the rewritten system; $\mathbf{F_{nl}^G}, \mathbf{F_e^G}$ are the nonlinear contact friction and external force vector. More details of the transformation leading to Eqn.3 can be referred to [36].

### *3.3. Reduced basis*

The reduced subspace of the rewritten system in Eqn.3 can be constructed with vibration modes $\phi$ of the linearised system and static modes $\psi$ related to internal variables $\Delta p$. The details to obtain these reduced basis can be referred to [36, 35]. With such a set of reduced basis, the transformation from the full physical coordinates to reduced subspace can be written as:

$$\begin{bmatrix} u \\ \Delta p \end{bmatrix} = \begin{bmatrix} \phi & \psi \\ \mathbf{0} & \mathbf{I} \end{bmatrix} \begin{bmatrix} \eta \\ \Delta p \end{bmatrix}, \tag{4}$$

where $\eta$ is the modal participation factors of the selected dynamic modes; $q$ is the reduced coordinates in the subspace. Most importantly, a second reduction can be carried out from Eqn. 4. It is obvious that the static modes associated to purely sticking contact nodes in $\Delta p$ can be removed from the reduced

subspace because $\Delta p$ would be zero for those sticking nodes. It can be easily achieved by only retaining the non-zero terms in $\Delta p$ in Eqn. 4. The transformation matrix for the second reduction can be expressed as:

$$\begin{bmatrix} u \\ \Delta p \end{bmatrix} = \begin{bmatrix} \phi & \psi \\ \mathbf{0} & \mathbf{I} \end{bmatrix} \begin{bmatrix} \mathbf{I} & \mathbf{0} \\ \mathbf{0} & \mathbf{B}_p \end{bmatrix} \begin{bmatrix} \eta \\ \Delta p_R \end{bmatrix} = \underbrace{\begin{bmatrix} \phi & \psi\mathbf{B}_p \\ \mathbf{0} & \mathbf{B}_p \end{bmatrix}}_{\Phi} \begin{bmatrix} \eta \\ \Delta p_R \end{bmatrix}, q = \begin{bmatrix} \eta \\ \Delta p_R \end{bmatrix} \tag{5}$$

where $\Delta p_R$ is the non-zero part of $\Delta p$; $\mathbf{B}_p$ is the Boolean matrix that helps to abstract on the non-zero part of $\Delta p$;$\Phi$ is the adaptive transformation matrix of the second reduced order model. The size of final ROM therefore can be related to the contact condition of the contact nodes. It is worth mentioning that such an adaptive ROM performs well in particular for a large number of nodes that remain in sticking condition, which is often the case for most jointed structures. Another advantage of adaptive ROM is that it can help immediately detect the friction nonlinearities by only observing the size of the adaptive ROM. Using the modal projection with $\Phi$, the reduced mass, stiffness, force matrix can be written as:

$$\mathbf{M^R} = \mathbf{\Phi}^T\mathbf{M^G}\mathbf{\Phi}, \mathbf{C^R} = \mathbf{\Phi}^T\mathbf{C^G}\mathbf{\Phi}, \mathbf{K^R} = \mathbf{\Phi}^T\mathbf{K^G}\mathbf{\Phi} \tag{6}$$

$$\mathbf{F_{nl}^R} = \mathbf{\Phi}^T\mathbf{F_{nl}^G}, \mathbf{F_e^R} = \mathbf{\Phi}^T\mathbf{F_e^G} \tag{7}$$

In the following section, it will be shown this reduced order model is used in the calculation of damped nonlinear modes, and also how the self-adaptive updating of this ROM is achieved with harmonic balance method.

## 4. Damped Nonlinear Normal Mode Calculation

This section is to describe the numerical method to calculate dNNMs, and also show the adaptive ROM is integrated into harmonic balance method for the computation of dNNMs.

### *4.1. Extended periodic motion concept*

The concept of extended periodic motion, which is originally proposed in [17], is adopted here to evaluate the dNNMs. Modal amplitude $\alpha$ is introduced to represent the modal energy in the nonlinear system as the modal properties of dNNM is dependent on the level of energy within the system. The solution of dNNM can be expressed as: $q(\alpha, t) = \alpha \cdot q_0(\alpha, t)$, where $q_0(\alpha, t)$ is normalised solution at modal amplitude of $\alpha$. In addition, the absolute phase of the solution in an autonomous system is arbitrary. Therefore, a mass normalisation and phase normalisation constraints are imposed in a similar way in [42]. The energy of the system is not constant due to the energy dissipation on friction contact and linear damping. The solution of dNNM is therefore not periodic. An artificial mass proportional modal damping is introduced into the system to make the motion of the system periodic as shown in Eqn.8. The aim of this artificial modal

damping is to balance the energy dissipated by frictional contact and the viscous damping within the linear system. $\omega_o(\alpha)$ is the amplitude dependent resonant frequency. $\eta(\alpha)$ is the equivalent damping ratio. Then, the equation to compute dNNMs using the adaptive reduced system can be rewritten as Eqn.9.

$$\mathbf{C_a} = -2\omega_o(\alpha)\eta(\alpha)\mathbf{M_R} \tag{8}$$

$$\alpha(\mathbf{M_R}\,\ddot{q_0}(\alpha,t) + \mathbf{C_a}\,\dot{q_0}(\alpha,t) + \mathbf{C_R}\,\dot{q_0}(\alpha,t) + \mathbf{K_R}\,q_0(\alpha,t)) + \mathrm{F}_{nl}^{R}(\Phi(\alpha q_0(\alpha,t))) = 0 \tag{9}$$

*4.2. Steady state response approximation*

Multi-harmonic balance method (HBM) is used to obtain the steady state reduced dynamic system from Eqn.9. The non-linear displacement $q(t)$ can be approximated by truncated Fourier series as:

$$q(t) = \tilde{Q}_0 + \sum_{i=1}^{n_h} (\tilde{Q}_i^c \cos m_i\omega_o t + \tilde{Q}_i^s \sin m_i\omega_o t) \tag{10}$$

where $\tilde{Q}_i^{c,s}$ are cosine and sine harmonic coefficients for $i^{th}$ harmonic; $\tilde{Q}_0$ is the zero harmonic coefficient; $n_h$ is the number of harmonics; $\omega_o$ is amplitude dependent resonant frequency. Using such an approximation, the size of original unknown vector is then expanded by $2n_h+1$ times. The framework of HBM includes three main components: Newton-Raphson solver, Alternating Frequency Time (AFT) procedure and continuation technique [6, 36, 43]. AFT technique is used to calculate the nonlinear contact friction force in time domain and transfer it to the frequency domain. The continuation technique is used to track the nonlinear dynamical response with tracking parameters. The modal amplitude $\alpha$ would be used as the tracking parameter in nonlinear modal analysis. The Secant method is used as the predictor and the arc-length method is for the corrector.

*4.3. Self updating algorithm*

The algorithm to update the size of reduced order model for nonlinear modal analysis is described in Algorithm 1. The classical continuation procedure within HBM framwork is kept unchanged. For each solution, the size of reduced basis is fixed and updated only when moving to compute the next solution. Before updating the reduced basis, contact friction force in an entire interface is evaluated for the current converged solution $\tilde{Q}^i$. The error estimator for each contact pair $e^i$ is then calculated in order to detect contact conditions of all nodes and then update the $\mathbf{B}_p^{i+1}$ with the pre-setting tolerance $\varepsilon$ [37]. $\mathbf{B}_p^{i+1}$ is used to update the reduced basis for the next modal amplitude $\alpha^{i+1}$. It means, for each continuation step, the reduced basis for the reduced system is updated by adding static modes related to slipping nodes to the reduced basis or removing static modes from those contact nodes in a sticking condition. Once the reduced basis is updated, the reduced basis will be used for the next continuation step and the size of the reduced system will remain constant. All the assumed slipping nodes from the last converged solution can be either in a sticking or slipping condition during a vibrational period. $\varepsilon$ needs to be defined beforehand based on

the allowable case-independent ratio of the energy dissipation level to the external energy level e.g. $10^{-10}$. In this case, three tolerance levels for the chosen test case are studied.

**Algorithm 1:** Adaptive size updating in the numerical continuation

**Result:** $[\tilde{Q}^1, \tilde{Q}^2, \ldots, \tilde{Q}^e], [\alpha^1, \alpha^2, \ldots, \alpha^e]$

Initial guess solution: $\tilde{Q}^0, \alpha^0, \mathbf{B}_p^0$

Initialization: $\alpha^1 = \alpha^0, \tilde{Q}^1 = \tilde{Q}^0, \mathbf{B}_p^1 = \mathbf{B}_p^0$;

**while** $\alpha^s \leq \alpha^i \leq \alpha^e$ **do**

Classical continuation:

(1) Predict: $(\tilde{Q}_p^i, \alpha_p^i) = f_{pre}(\tilde{Q}^{i-1}, \alpha^i)$;

(2) Correct: $(\tilde{Q}_c^i, \alpha_c^i) = f_{cor}(\tilde{Q}_p^i, \alpha_p^i, \mathbf{M}_R, \mathbf{K}_R, \mathbf{\Phi}, \mathbf{B_p^i})$;

Expand and save: $(\tilde{Q}^i, \alpha^i) = f_{expand}(\tilde{Q}_c^i, \alpha_c^i, \mathbf{B_p^i})$;

Contact condition re-evaluation to update AROM:

(1) Call $F_{nl}(\tilde{Q}^i, \mathbf{\Phi})$ to calculate friction force of entire interface nodes;

(2) Evaluate the error estimator $e^i$ for each interface node $i$;

(3) Update $\Delta p^i$ with $e^i$ for each contact node $i$;

(4) Obtain $\mathbf{B}_p^{i+1}$ for non-zero part in updated $\Delta p$;

**if** $\mathbf{B}_p^{i+1} \neq \mathbf{B^i}_p$ **then**

Update reduced system $\mathbf{M}_R, \mathbf{K}_R, \mathbf{\Phi}$ with $\mathbf{B}_p^{i+1}$ (Eqn.5 and Eqn.6);

Update the size of the converged solution $\tilde{Q}^i$ with $\mathbf{B}_p^{i+1}$;

**end**

i=i+1;

**end**

## 5. Forced response interpolation from dNNMs

The calculation of steady state dNNMs using the adaptive ROM have now been described. This section is to present the numerical methods for forced response reconstruction from the dNNMs. Two methods are considered here: one is E-EBM to predict forced resonant response; the other is nonlinear mode synthesis method to reconstruct the full FRFs.

### *5.1. Forced resonant response prediction*

The dNNM is regarded as a collection of resonant solutions in the forced response. However, it is not immediately clear to relate the dNNMs to resonant response at different excitation positions. The E-EBM is applied to predict the resonance. The idea of this method consists in the fact that the total energy transferred into a system within one period must be zero. The resonant solution of forced response is similar

to that of the dNNM, for small enough forcing and damping, the solutions are assumed to be identical. It means that when the excitation frequency $\Omega$ coincides with amplitude dependent resonant frequency $\omega_o$, the resonant solutions in forced response $q_f$ are assumed to be same as the dNNM with a certain level of modal amplitude $q = \alpha \cdot q_0(\alpha)$. The solutions are named as 'resonant shared solutions '($\chi$).

$$\chi = q \approx q_f, \text{when } \Omega = \omega_o(\alpha) \tag{11}$$

$$E_d = \int_0^{2\pi/\omega_o(\alpha)} (\mathbf{C}^R + 2\omega_o(\alpha)\eta(\alpha)\mathbf{M}^R) \cdot \dot{\chi} \cdot \dot{\chi} dt \tag{12}$$

$$E_f(\gamma, \varphi) = \int_0^{2\pi/\Omega} \mathrm{F}_e(\gamma, \varphi, \Omega, t) \cdot \dot{\chi} dt \tag{13}$$

The energy dissipation $E_d$ can be then calculated by integrating the product of artificial damping force in Eqn.8 and displacement over one vibration period $2\pi/\omega_o(\alpha)$ as shown in Eqn.12. Similarly, the external excitation energy $E_f(\gamma, \varphi)$ can also be integrated, whereas $E_f$ varies with forcing level $\gamma$ and forcing phase $\varphi$ as shown in Eqn.13. To determine the value of $\gamma$ and $\varphi$, a single intersection between the curve of $E_f$ ($E_f$ against $\varphi$) and the constant $E_d$ will occur at the maximum position. This process is applied to each value of modal amplitude $\alpha$ and the corresponding force amplitude at the selected excitation position can be constructed.

### *5.2. Full forced response reconstruction*

The full nonlinear FRFs can also be reconstructed from the nonlinear modes using single nonlinear resonant mode theory [20]. We assume that only the $j^{th}$ mode dominates the nonlinear vibration behavior of the system while the remaining modes are linearised. However, the nonlinear mode can only accurately reconstruct the forced response close to the resonant frequency. To increase the accuracy for the response away from the resonance, the linear correction terms from other linear modes are needed. Therefore, the forced frequency response can be synthesised between the nonlinear mode and other linearised modes as [21]:

$$u(t) = \alpha(\Omega)\Psi_j(\alpha(\Omega))(t) + \sum_{i \neq j} \Phi_i \eta_i(\Omega, t) \tag{14}$$

Where u(t) is the forced response of the system; $\Omega$ is the external excitation frequency; $\Psi$ is denoted as the dNNM from nonlinear modal analysis, which is namely $q_o(t)$ shown from Eqn.10; $\Phi$ includes the linearised modes in reduced basis. The modal amplitudes $\eta_i$ can be directly computed through the modal superposition method by using the projected linearised systems. The modal amplitude of the nonlinear mode is determined independently of the linear modes and by only considering the fundamental harmonic in nonlinear mode $\Psi_j$ in the multiharmonic expansion of the nonlinear mode. This method is referred as nonlinear modal synthesis (NMS) in this paper.

## 6. Test case

### *6.1. Fan blade system*

Fan blade system is the largest bladed disc assembly in a modern turbofan engine that provides the over 60% thrust to propel the aircraft [44, 30]. This fan assembly consists of a number of blades and a disc on the rotating shaft. They are commonly assembled through a disk via curved or straight dovetail roots. Such a design ensures easy assembly and safe load distribution, and also provides essential damping to the system. The state-of-the-art linear vibration analysis often leads to an over-design of the components by ignoring the non-linearities from the dovetail joint due to the complex and strong nonlinear dynamic nature in the friction joint. To further improve the fan blade root design, it is therefore necessary to take these non-linearities into account for a better dynamic design [45]. However, performing non-linear dynamic analysis for a large-scale system remains as an academic and industrial challenge partly due to the heavy computational expense. For these reasons, this large-scale fan blade system is used as the test case in this paper.

### *6.2. Industrial-scale FE model*

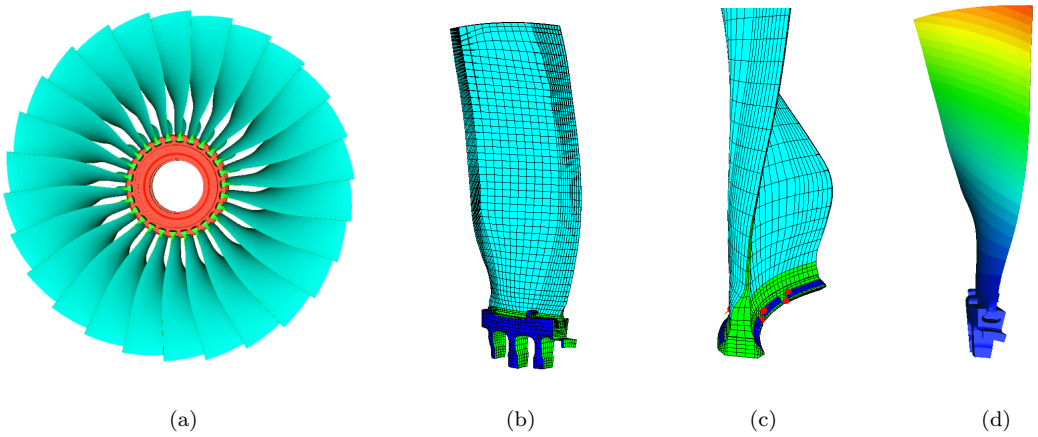

(a) (b) (c) (d)

Figure 2: (a) Fan system assembly (b) One fan sector (c) Dovetail joint (d) First bending mode

Figure.2a shows a full scale fan blade system in turbofan aero-engine that includes more than two dozens of blades (in blue) and one disc (in red) connected via curved dovetails joints. The fan blade system is cyclic symmetric, and one sector of the assembly is therefore considered for this study. Figure.2b shows a sector of the bladed disc assembly where the deep blue part of the disc is the cyclic boundary. The blade has a low slenderness aspect ratio of around 4 and an increasing twist from root to tip. This high fidelity finite element model was built with the quadratic hexahedral element and each node has 3 DOFs. The model of each sector consists of a blade of 27,707 nodes and a cyclic symmetric part of the disc of 13,826 nodes. Figure.2c show the geometry of a blade with a curved root that connects the disc. The matching mesh (node to node) is used on the contact interface that allows the use of 3D node to node contact element, which has

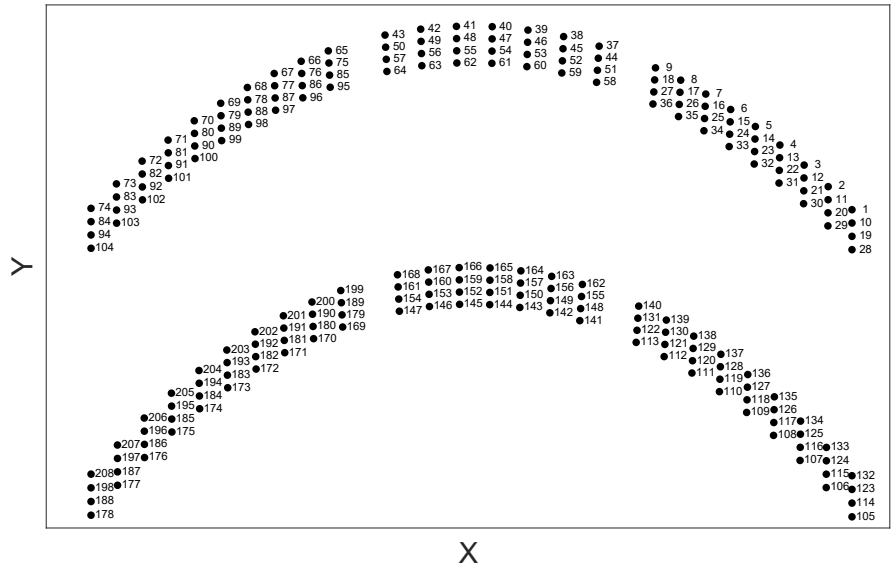


Figure 3: 2D projection contact nodes in dovetail joint

been detailed in section 3.1. Figure.2d shows the first flapping mode of the fan blade sector, which would be further studied for nonlinear modal analysis using adaptive ROM. Figure 3 shows a X-Y plane projection of 208 contact node pairs in the curved contact interface with their numbering. There are in total $208 \times 6$ contact friction DOFs. For each of the contact pair, a local coordinate system will be created due to the nature of curved contact interface.

## 7. Results

### *7.1. The property of dNNMs*

The dNNMs are computed using the numerical methods explained above. Figure 4a shows the evolution of resonant frequency $\omega_o$ and damping ratio $\eta$ against modal amplitude $\alpha$ . By looking at the red curve in Fig.4a, the resonant frequency $\omega_o$ is constant when modal amplitude is smaller than 0.015 and starts to decrease when $\alpha \geq 0.015$. As for dissipated damping $\eta$, the similar turning point can be found. The dissipated damping $\eta$ is null for low modal amplitude ($\alpha < 0.015$). A positive dissipated damping $\eta$ can be obtained when $\alpha$ is larger than 0.015. Such a linear behavior at low modal amplitudes is because all the contact nodes remain in a sticking condition. The system can be regarded as an equivalent linearised system. A further increase of modal amplitude would initiate the sliding contact status and a typical softening effect can be seen due to the transition of contact status (from sticking to sliding). The sliding contact nodes lead to an energy dissipation and a softening effect resulting in a decrease in resonant frequency. It is worth noting that, although bladed disc systems have high modal density and many modes can appear in a narrow frequency band, damped nonlinear modal analysis can be still applied and used as a effective tool to track

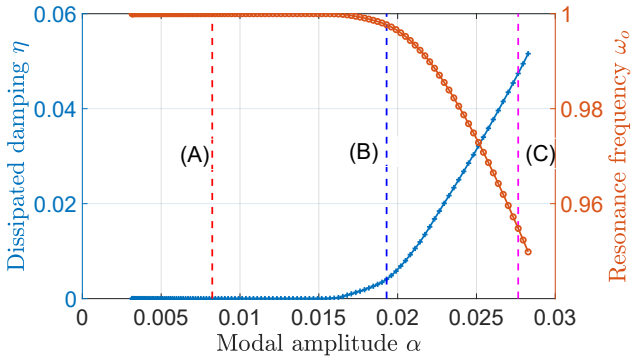


(a) Resonant frequency and damping

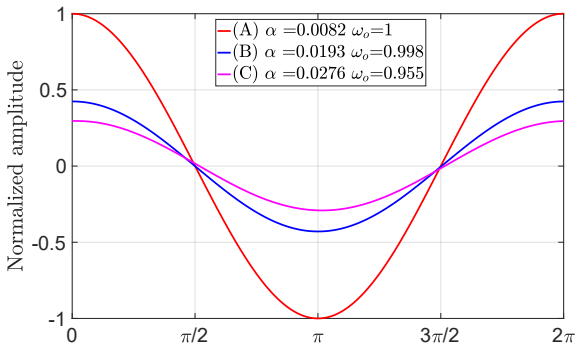


(b) Steady state response in a period

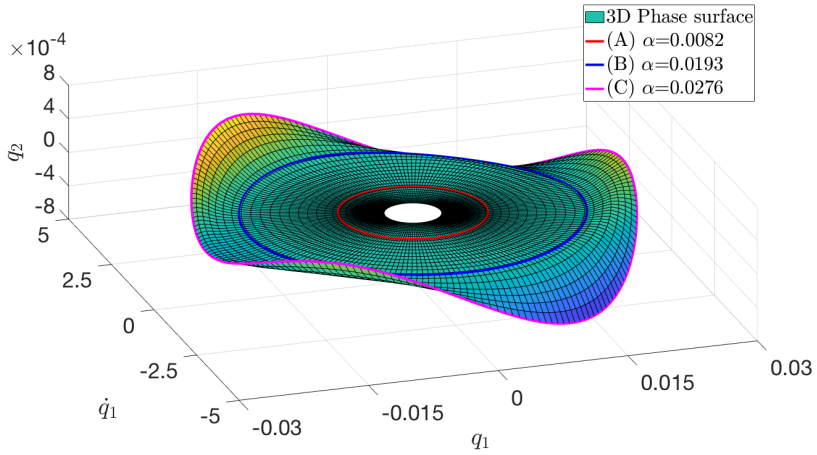


(c) Invariant manifold: mode1 and mode2

Figure 4: (a) Resonant frequency and damping at different modal amplitudes (b) Steady state response of three cases on the blade tip over a period (c) 3D invariant manifold

the resonance in the forced response, since most of the time only one mode dominates the response [42]. For a mistuned system, the application of nonlinear modal analysis can be challenging, especially when there is a nonlinear coupling between modes. Otherwise, the nonlinear modal analysis can still be applied as demonstrated in [46].

To further demonstrate the nonlinear modes, three solutions at different modal amplitude ($\alpha = 0.0082$, 0.0193 and 0.0276) are selected as demonstration cases A, B and C. Figure. 4b shows the steady state response from the blade tip in these three cases over a period where the amplitude is normalized by the linear case. As is shown in Fig.4a, case A is considered as a linear case where the equivalent damping ratio $\eta = 0$ and normalized resonant frequency $\omega_o = 1$. The resonant amplitude of blade tip reaches maximum among the three selected cases. Where as for Case B, the system starts to behave non-linearly with higher

modal amplitude. $\eta$ is increased to 0.005 and $\omega_o$ drops to 0.996. It also leads to lower resonant response amplitude to 0.42. With the increase of $\alpha$ to 0.0276, case C has a $\eta$ of 0.016 and $\omega_o$ of 0.955. The resonant amplitude for case C is reduced further from 0.45 to 0.3. The case B and case C will be further investigated later.

Fig.4c shows a 3d invariant manifold of the system with modal coordinates $q_1$-$\dot{q}_1$-$q_2$, where $q_1$ is the modal coordinate of the first linearised mode; $\dot{q}_1$ is the velocity of the $q_1$ and $q_2$ is that of the second linearised mode. This 3D invariant manifold is part of the first nonlinear mode of fan blade systems. This hypersurface as a part of invariant manifold is constructed using a collection of damped periodic solutions from the calculated dNNMs over a period. The periodic solutions for above-mentioned three demonstrated cases (A, B and C) are also highlighted in different colors. At low modal amplitudes, the system behave linearly where the periodic motions stay in the flat plane in the center of the manifold where $q_2$ stays at zero for all the points. It means that there is not any contribution from the second mode, e.g. linear Case (A). When the modal amplitude reaches 0.019, e.g. Case (B), the flat plane cannot be held anymore and it starts to be twisted which means the second mode starts to couple with the first mode due to the contact friction non-linearities. With a further increase of modal amplitude as Case (C), the phase surface is further twisted, and one can clearly see the surface bends inward and outward. The modal amplitude of the second mode increases to 0.05%. It means the coupling between first two modes becomes stronger however the first mode still dominates the dynamic response.

### *7.2. Comparison of AROM and CB method*

This section is to compare the dNNMs computed from AROM and classical CB method. The property of resonant frequency and damping ratio between these two methods is firstly compared; then, we present the comparison of the contact condition and energy dissipation on the contact interface; it is then followed by a comparsion of computational cost.

#### *7.2.1. Resonant frequency and Damping*

Figure.5 shows a comparison of resonant frequency and dissipated damping ratio. The solid lines are the results from CB method while the dashed lines are from the adaptive ROM. For the adaptive ROM, the results are computed using 3 different tolerance levels defined in error estimator to automatically select static modes from contact interface, which are $1e-20, 1e-10$ and $1e-2$. One can clearly see that, when the tolerance equals to $1e-20$, the resonant frequency and damping ratio from adaptive ROM completely overlays the results from classical CB method. When the tolerance increases to $1e-10$, the discrepancies of resonant frequency and damping ratio can be clearly observed when the modal amplitude is larger than 0.024. As expected, the difference between AROM and CB becomes larger (up to 5%) when the modal amplitude increases further. The results from the tolerance of $1e-2$ do not show much difference compared to that with tolerance of $1e-10$. The difference however appears early from modal amplitude around 0.02.

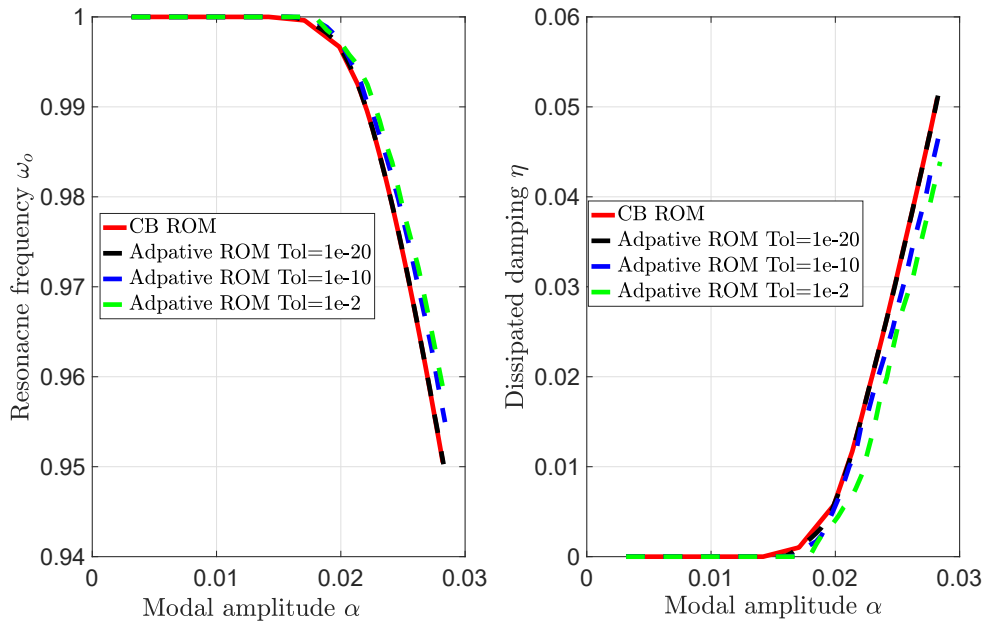


Figure 5: Comparison of nonlinear modal properties between adaptive ROM and CB method

### *7.2.2. Contact status and energy dissipation*

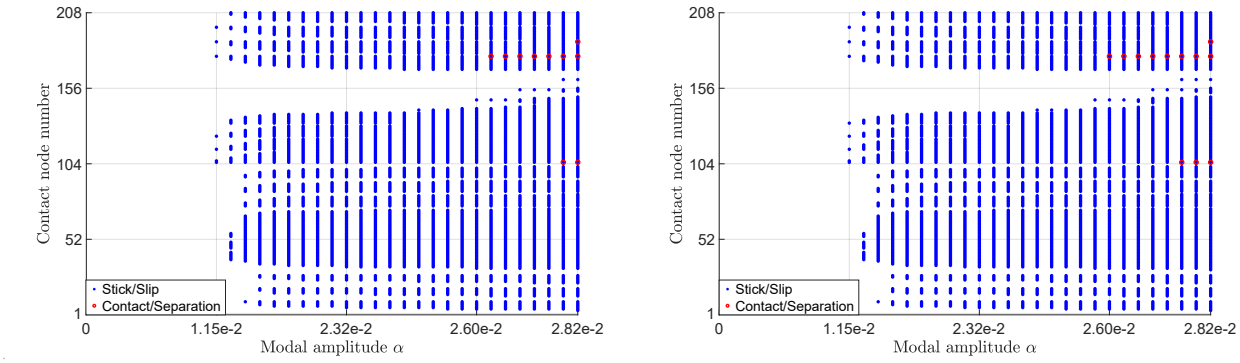


Figure 6: Contact status with (a) Adaptive ROM method (b) CB method

Figure.6 shows a comparison of the contact conditions for each interface nodes at different modal amplitudes between adaptive ROM (Tol=1e-20) and CB method. The contact node number in Y axis is consistent with the node numbering shown in Fig.3. The blue color represents the stick-slip condition on that node while the red color means the contact-separation condition. It shows that the contact condition of dNNM computed by adaptive ROM is almost same as that computed by CB method. The slipping and separation condition of both dNNMs start at the same modal amplitude around $1.15e-2$ and $2.60e-2$. The slipping

and separating nodes from CB method appear a bit early than that from adaptive ROM. For example, at the modal amplitude of $1.15e-2$, the number of stick-slip nodes from CB method is 8 while that from adaptive ROM is 7. At the modal amplitude of $2.60e-2$, the number of contact/separation node from CB method is 1 while that from adaptive ROM is 0.

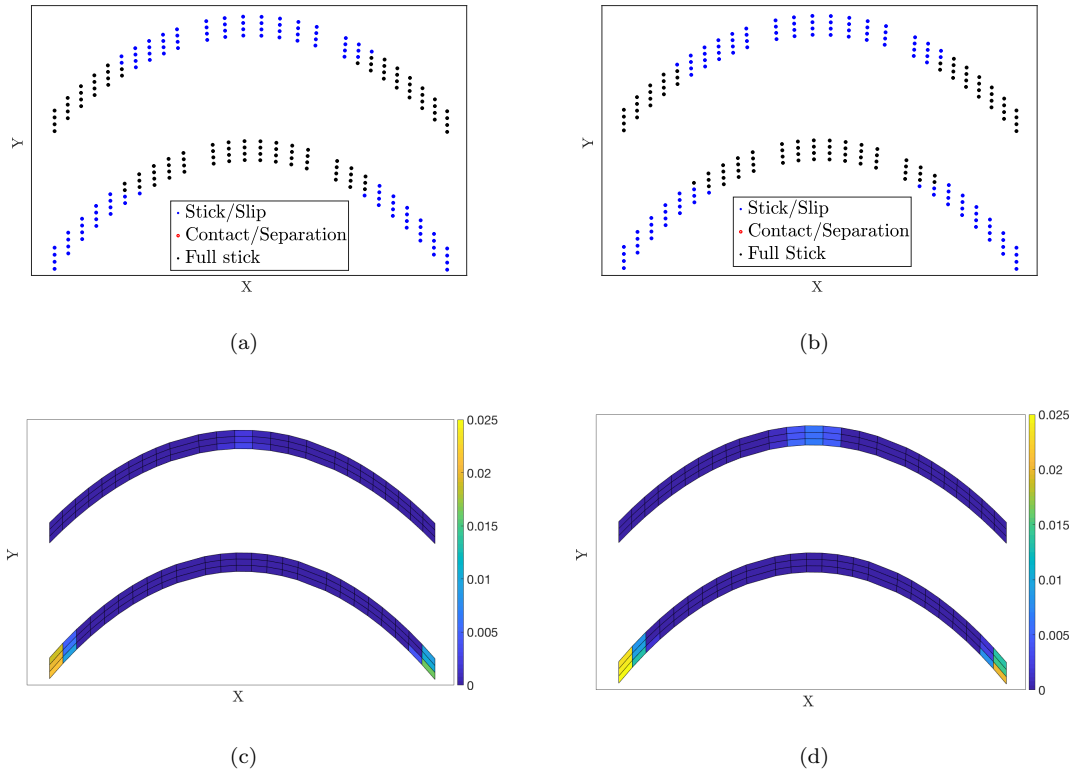


Figure 7: Case (B): (a,b) Contact status; (c,d) Dissipated energy; (a,c) AROM method; (b,d) CB ROM method

To give more insights into dNNMs computed from adaptive ROM (Tol=1e-20) and CB method, Figure.7 and 8 show the distribution of the contact condition and also dissipated energy on the 2D projected contact interface at different modal amplitudes. Figure.7 compares these nonlinear properties at modal amplitude of 0.019 (namely Case B) while Fig.8 at modal amplitude of 0.028 (namely Case C). At modal amplitude of 0.019, the contact nodes start to slip from the edges in the bottom contact interface while from the center in the top contact interface. They then propagate to the centre of bottom interface and to the edges of top interface at a high amplitude. The separation condition only appears at a high amplitude. The energy dissipation follows the same propagation trend as the slipping contact nodes. It can be clearly seen that both Case B and Case C generally show a very good agreement on the distribution of contact conditions and dissipated energy between adaptive ROM and CB method. There is a slight difference (around 1%) in the energy dissipation levels in Case B and Case C. This further validates the accuracy of the adaptive ROM for the computation of dNNMs.

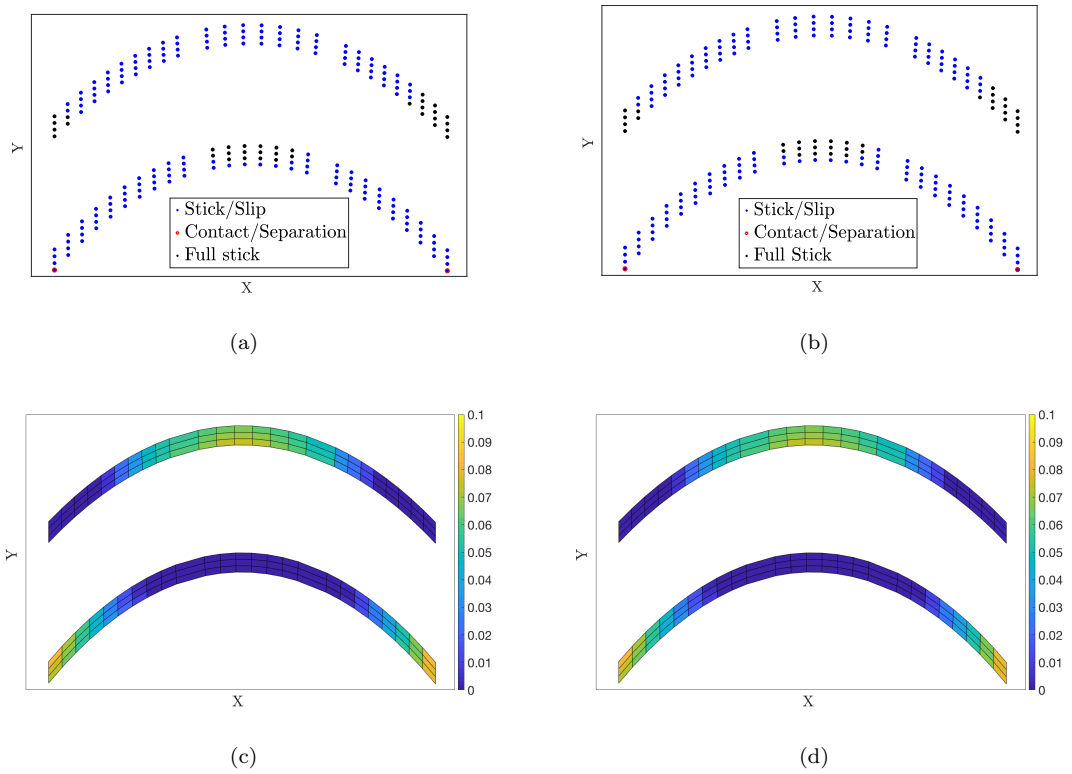


Figure 8: Case (C): (a,b) Contact status; (c,d) Dissipated energy; (a,c) AROM method; (b,d) CB ROM method

### *7.2.3. Computation cost*

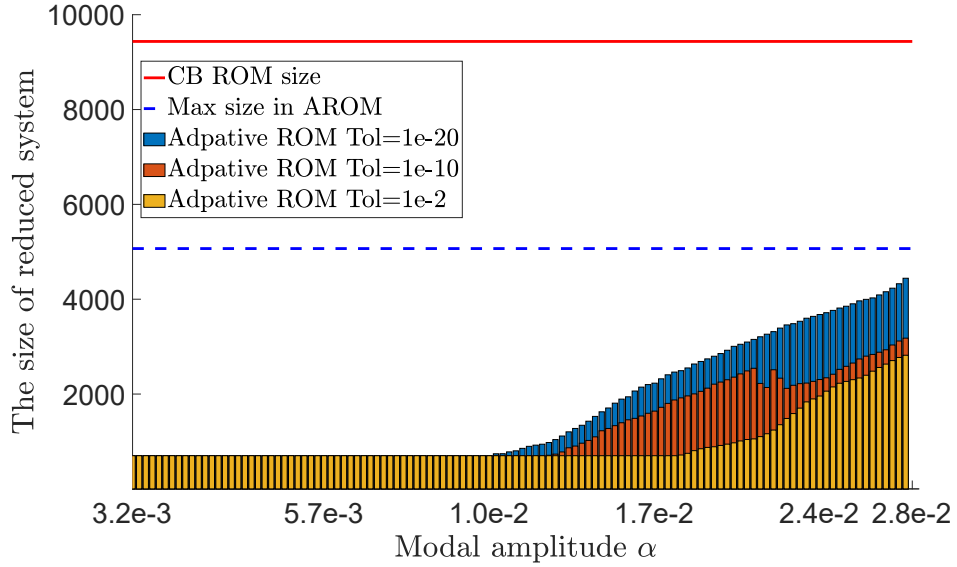


Figure 9: Comparison of system size between AROM and CB ROM

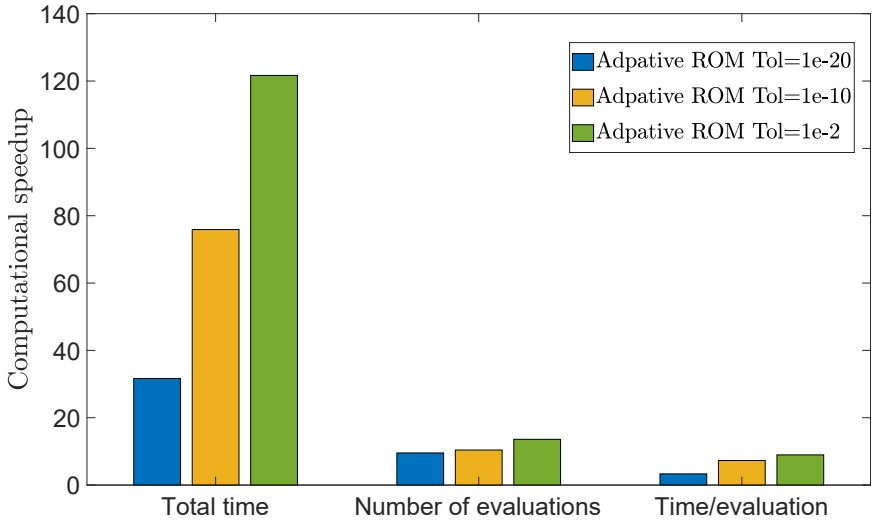


Figure 10: Compuational speedup of AROM against CB ROM

Figure.9 compares the size of adaptive ROM and classical CB method during the computation of dNNMs at different modal amplitudes. The red line is the size of CB model, which remains constant for all the modal amplitude. The dashed blue line is the maximum size of adaptive ROM, which would occur when all the contact nodes are in the slipping condition. The maximum size of adaptive ROM is around the half of CB model as size of the full internal variable is half number of the static modes used in CB model. The size of adaptive ROM with three tolerance levels $(1e-20, 1e-10, 1e-2)$ are plotted as bars in Fig.9. As expected, the size of adaptive ROM keeps minimum in the linear region when the modal amplitude is less than $1.0e-2$. The minimum size of adaptive ROM is 100 (the number of linearised modes) times $2*n_h+1$ where $n_h$ is the number of harmonics (nh=3 in this case). After that, the size of adaptive ROM slowly increases with the growth of the modal amplitude. The adaptive ROM with lowest tolerance (Tol=$1e-20$) can firstly detect the slipping nodes but has the largest size compared to the other two adaptive ROM with lower levels of tolerance at high modal amplitudes. As expected, the size of the system increases with the modal amplitude as the number of slipping nodes increases for both tolerance levels (Tol=1e-20 and 1e-2). However, for Tol=1e-10, there is a slight decrease in the reduced system size around $\alpha = 2.1e-2$. The main reason for this change in size is the numerical noise. In the transition period between micro-slip and macro-slip when the energy dissipation of stick-slip nodes is close to the pre-setting tolerance level the system is very perceptive to noise, while once elements are slipping, this noise dependence drops, and hence the system size increases somewhat less. From the case study, it is clear that the adaptive approach is more efficient when a large number of nodes remain in a sticking condition. The proposed approach therefore is particularly useful for jointed structures where most of contact nodes are normally in a sticking condition. However, it does not mean that the accuracy of the proposed method would be reduced when the interface

is in a marcoslip condition as shown in the case study at a high modal amplitude. The accuracy of adaptive ROM would remain same as CB method even when only a small portion of nodes is coupled.

Figure.10 shows the speed up of using adaptive ROM at different tolerance levels for the computation of dNNMs against counterpart of CB method. It also includes the number of evaluations and average speed up of adaptive ROMs with these three tolerance levels. Consistent with the system size shown in Fig.9, the adaptive ROM with a high tolerance level always leads to an overall high computational speedup. The speed up increase from 32 to 120 when the tolerance level grows from 1e-20 to 1e-2. It is worth noting here, even with a lowest tolerance level of $1e-20$, the adaptive ROM can achieve a speedup of 32 while the loss of the accuracy is almost null as shown in Fig.5. Obviously, high speed up would compromise the accurate prediction of dNNMs. The use of tolerance of $1e-2$ in adaptive ROM underestimates the resonant frequency by around 5-10% as discussed in Fig.5. In terms of number of evaluations, the first two adaptive ROMs with low tolerance level remains similar size while the third one has slight higher number of nonlinear evaluations. The average speed up per evaluation for three adaptive ROM are 3.32, 7.29 and 8.95.

### *7.3. Prediction of forced response using dNNMs*

This section is to show the forced response predictions from dNNMs that are previously obtained from the adaptive ROM. Energy balance method and nonlinear modal synthesis are used to predict resonant response and also full FRFs separately. These predictions are then compared with directly computed FRFs using CB method. The accuracy and computational time from these predictions will be demonstrated.

#### *7.3.1. Forced resonant response interpolation*

Using the E-EBM as described in 5.1, the excitation forcing level can be predicted for each solution along dNNMs at each modal amplitude. The solution from dNNM can be considered as resonant solution in a forced response with the predicted excitation forcing level. In Fig.11a, the evolution of excitation forcing level $F$ is plotted against the forced resonant amplitude from the blade tip. To validate the predicted excitation forcing level, six nonlinear forced responses are computed for different values of excitation forcing level ($F = 1\ N$, $3\ N$, $5\ N$, $8\ N$, $10\ N$ and $12\ N$). Using amplitude-force curve, for given excitation forcing level, the corresponding vibration amplitude are marked by different colors on the left hand side of Fig.11a. Whereas on right hand side of Fig.11a, the actual resonant amplitude from nonlinear forced responses are compared with the predicted amplitude on the left.

Figure.11b also shows the 3D view of interpreted dNNM and nonlinear forced response are provided in a $\omega$-$F$-Amplitude space. The predicted resonances by E-EBM have a good agreement with the actual resonance from nonlinear forced response. This means that the forced resonant response from any excitation location in the structure can be directly and accurately interpolated from the dNNM with almost null computational cost. The time-consuming forced frequency response simulations can be saved.

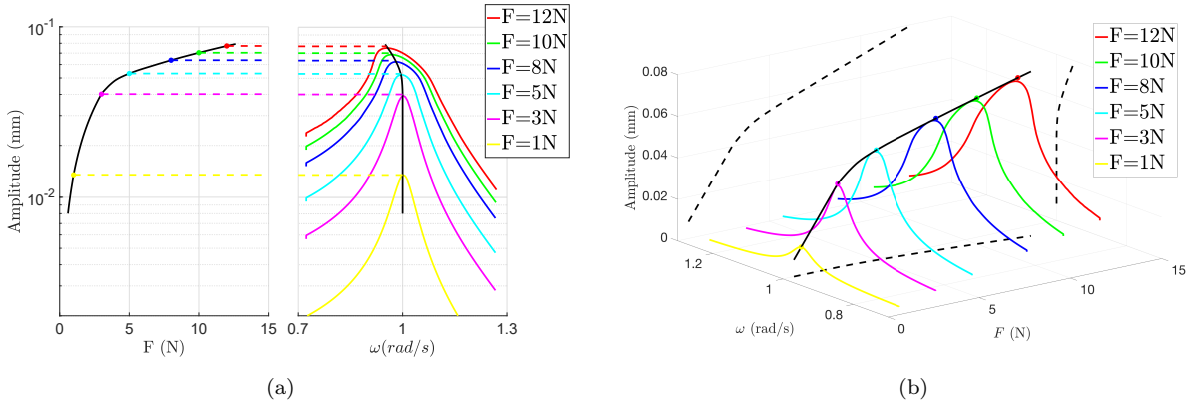


Figure 11: (a) 2D Nonlinear modes and FRFs (b) 3D Nonlinear modes and FRFs

### *7.3.2. Full synthesised forced response*

The nonlinear forced response can be also reconstructed using nonlinear mode synthesis as shown in Eqn.14. Fig.12 shows the comparison between reconstructed forced response (black dashed) from dNNMs and numerically computed forced responses at different excitation levels. In general, the reconstructed forced response can well capture the forced frequency response. At low excitation forcing levels ($F$ = 1 $N$, 3 $N$ and 5 $N$), the reconstructed forced response overlay on the actual forced response without any visible differences. Whereas, for large excitation forcing level, there are some discrepancies between the reconstructed forced response and the actual one near resonance. Such a discrepancy becomes large when the excitation level increases from 8N to 12N. This is mainly because only the fundamental harmonic is used to obtain corresponding modal amplitude for the nonlinear mode while the influence of higher order harmonics on the dynamics are ignored, leading to some errors in the resonant response. The other reason for an overestimation in reconstructed FRFs is that the contributions of other linearised modes to the resonant response is doubled accounted in Eqn.14. The forced response from the single nonlinear mode itself includes contributions from other modes near the resonance. However, the linear correction terms from modal superposition also added the contribution from other linear modes close to the resonant frequency. Therefore, the reconstructed forced responses have been found less accurate for large excitation forcing level near resonance.

### *7.3.3. Computational time*

Table 1 shows a comparison of CPU time between interpolated forced response from dNNMs and the forced response from direct computations. As it is shown in Table 1, once the dNNMs is computed, the computational cost for resonant response prediction using E-EBM is almost null for all the excitation levels. The computational time for a whole FRF reconstruction (for a frequency between 0.72 and 1.27) remains almost constant around 22s, even at very high excitation levels. It is because, with the help of single resonant

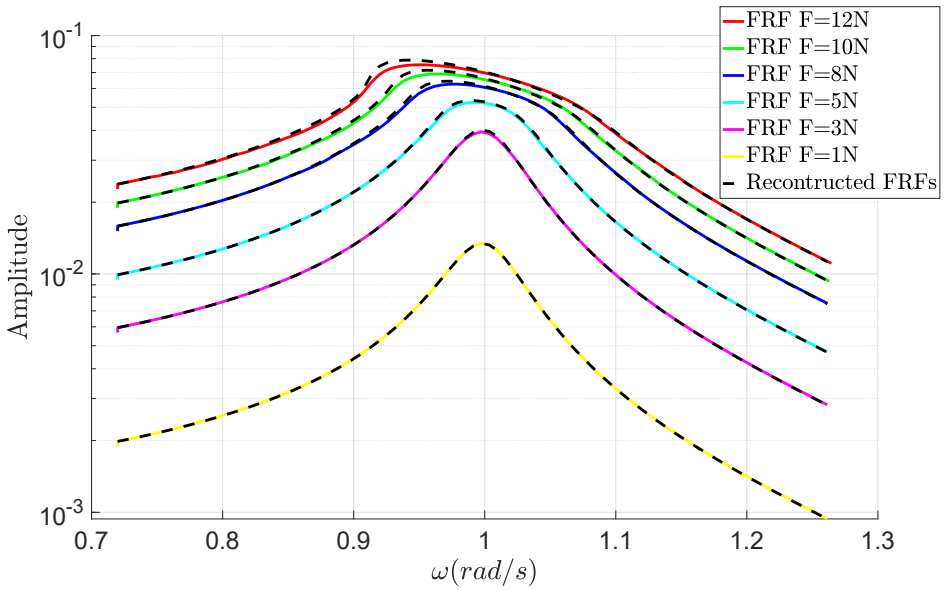


Figure 12: Reconstructed FRFs from dNNMs

mode theory, the nonlinear system is converted into a linear system through the change of coordinates in the phase space as shown in Fig.4c. In comparison, the computational cost from the direct force response increases significantly when the excitation levels become large. For example, at the excitation of 12N, the computing of direct FRF simulation is 100 times higher than that from interpolated forced response (given that dNNMs has been computed). Certainly, the forced response interpolation requires a off-line computation of dNNMs while direct forced response does not need to. However, the computation of dNNMs is one off and it can be used to interpolate any forced response wherever the excitation location is and however large the excitation amplitude is. If we only look at the total computation time of these 6 FRFs, the speedup of interpolated method against the dircet FRF simulation is around 2.

Table 1: Comparison of computational time between interpolated forced response and directly computed ones

| **Method** | **Type** | **dNNM calculation** | **F=1N** | **F=3N** | **F=5N** | **F=8N** | **F=10N** | **F=12N** | **Total time** |
|---|---|---|---|---|---|---|---|---|---|
| Predicted from dNNMs | **E-EBM**: Resonance | 2540s | $\approx 0s$ | $\approx 0s$ | $\approx 0s$ | $\approx 0s$ | $\approx 0s$ | $\approx 0s$ | 2540s |
| | **NMS**: Full FRFs | 2540s | 24s | 21s | 23s | 21s | 23s | 24s | 2676s |
| Directly computed | Full FRFs | Not needed | 182s | 185s | 222s | 409s | 2012s | 2218s | 5228s |

## 8. Conclusions

The main objective of this work was to improve the computation of dNNMs in a large scale nonlinear system with friction joints. It was achieved by employing an advanced adaptive ROM technique leading to a significant size reduction of the model using classical ROMs. This study described a detailed implementation of this adaptive ROM for the calculation of damped nonlinear modes using multi-harmonic balance method.

The accuracy and computational merits of the dNNMs computed by the adaptive ROM is benchmarked by classical Craig Bampton method.

An industrial-scale fan blade system with a large size of contact interface was used as a test case. The dNNMs based on the concept of extended periodic motion was successfully computed using a frequency domain solver. Compared to classical CB method, the resonant frequencies and modal damping from adaptive ROM method are very accurate in a wide range of modal amplitude. It can also make the computation of damped nonlinear modes at least 20 times faster than the reference CB method. The sensitivity study of tolerance levels also showed the computing speedup from the adaptive ROM can be further increased to 120 with a loss of accuracy only 5%.

The other contribution of this paper is that it proved that the dNNMs can be effectively used to predict the forced response for a large scale system through nonlinear modal synthesis and energy balance method. The study showed both forced resonance responses and whole FRFs at different excitation levels can be effectively interpolated from the dNNMs. In comparison to directly computed FRFs from CB method, the maximum relative error of interpolated forced response in the resonance is less than 1%. It further validated the accuracy of the dNNMs computed by the adaptive ROM. We also found that the computational cost of nonlinear modal synthesis was very tiny and remain almost constant for all forcing levels. For example, the synthesized FRF at the force level of 12N is 100 times faster than that computed from direct FRF simulations. Such a cheap computation cost would be much appreciated when a large number of FRFs are needed to compare with experimental results.

Overall, the study confirms that the novel adaptive ROM can be effectively used for the fast computation of dNNMs in a large scale system with friction joints. It can significantly reduce the computational cost to a readable level while maintain high accuracy of resulting modal properties.

## 9. Acknowledgements

The authors would like to acknowledge the support of Rolls-Royce plc through the Vibration University Technology Centre (UTC) at Imperial College London, UK. Dr.Jie Yuan and Dr.Christoph Schwingshackl acknowledge financial support from the EPSRC under SYSDYMATS project, Grand Ref: EP/R032793/1. Dr.Loïc Salles thanks Rolls-Royce plc and the EPSRC for the support under the Prosperity Partnership Grant "Cornerstone: Mechanical Engineering Science to Enable Aero Propulsion Futures", Grant Ref: EP/R004951/1. We also thank Dr.Ludovic Renson from Imperial College London for very useful discussion and suggestions on the paper.

## References

[1] G. Kerschen, M. Peeters, J.-C. Golinval, A. F. Vakakis, Nonlinear normal modes, part i: A useful framework for the structural dynamicist, Mechanical systems and signal processing 23 (1) (2009) 170–194.

[2] R. J. Kuether, L. Renson, T. Detroux, C. Grappasonni, G. Kerschen, M. S. Allen, Nonlinear normal modes, modal interactions and isolated resonance curves, Journal of Sound and Vibration 351 (2015) 299–310.

[3] L. Renson, G. Kerschen, B. Cochelin, Numerical computation of nonlinear normal modes in mechanical engineering, Journal of Sound and Vibration 364 (2016) 177–206.

[4] C. Schwingshackl, E. Petrov, D. Ewins, Measured and estimated friction interface parameters in a nonlinear dynamic analysis, Mechanical Systems and Signal Processing 28 (2012) 574–584.

[5] R. Lacayo, L. Pesaresi, J. Groß, D. Fochler, J. Armand, L. Salles, C. Schwingshackl, M. Allen, M. Brake, Nonlinear modeling of structures with bolted joints: A comparison of two approaches based on a time-domain and frequency-domain solver, Mechanical Systems and Signal Processing 114 (2019) 413–438.

[6] M. Krack, L. Salles, F. Thouverez, Vibration prediction of bladed disks coupled by friction joints, Archives of Computational Methods in Engineering 24 (3) (2017) 589–636.

[7] Y. Sun, J. Yuan, L. Pesaresi, E. Denimal, L. Salles, Parametric study and uncertainty quantification of the nonlinear modal properties of frictional dampers, Journal of Vibration and Acoustics 142 (5).

[8] Z. Li, H. Ouyang, Z.-H. Wei, Insights into instability of friction-induced vibration of multi-degree-of-freedom models, Journal of Sound and Vibration (2021) 116107.

[9] J. Yuan, F. El-Haddad, L. Salles, C. Wong, Numerical assessment of reduced order modeling techniques for dynamic analysis of jointed structures with contact nonlinearities, Journal of Engineering for Gas Turbines and Power 141 (3) (2019) 031027.

[10] M. R. W. Brake, J. Groß, R. M. Lacayo, L. Salles, C. W. Schwingshackl, P. Reuß, J. Armand, Reduced Order Modeling of Nonlinear Structures with Frictional Interfaces, Springer International Publishing, Cham, 2018, pp. 427–450.

[11] A. Kelley, On the liapounov subcenter manifold, Journal of Mathematical Analysis and Applications 18 (3) (1967) 472–478.

[12] A. M. LYAPUNOV, The general problem of the stability of motion, International Journal of Control 55 (3) (1992) 531–534.

[13] R. M. Rosenberg, Normal modes of nonlinear dual-mode systems, Journal of Applied Mechanics 27 (2) (1960) 263–268.

[14] S. W. Shaw, C. Pierre, Non-linear normal modes and invariant manifolds, Journal of Sound and Vibration 150 (1) (1991) 170–173.

[15] D. Laxalde, L. Salles, L. Blanc, F. Thouverez, et al., Non-linear modal analysis for bladed disks with friction contact interfaces, in: ASME Turbo Expo 2008: Power for Land, Sea, and Air, American Society of Mechanical Engineers Digital Collection, 2008, pp. 457–467.

[16] M. Krack, Nonlinear modal analysis of nonconservative systems: extension of the periodic motion concept, Computers & Structures 154 (2015) 59–71.

[17] M. Krack, Nonlinear modal analysis of nonconservative systems: Extension of the periodic motion concept, Computers & Structures 154 (2015) 59–71.

[18] D. Laxalde, F. Thouverez, Complex non-linear modal analysis for mechanical systems: Application to turbomachinery bladings with friction interfaces, Journal of Sound and Vibration 322 (4) (2009) 1009–1025.

[19] M. Jahn, S. Tatzko, L. P. von Scheidt, J. Wallaschek, Comparison of different harmonic balance based methodologies for computation of nonlinear modes of non-conservative mechanical systems, Mechanical Systems and Signal Processing 127 (2019) 159–171.

[20] W. Szemplińska-Stupnicka, The modified single mode method in the investigations of the resonant vibrations of non-linear systems, Journal of Sound and Vibration 63 (4) (1979) 475–489.

[21] M. Krack, L. Panning-von Scheidt, J. Wallaschek, C. Siewert, A. Hartung, Reduced order modeling based on complex nonlinear modal analysis and its application to bladed disks with shroud contact, Journal of Engineering for Gas Turbines and Power 135 (10).

[22] A. grolet, On a model reduction method for computing forced response using non-linear normal modes, working paper or preprint (Oct. 2019).
URL `https://hal.archives-ouvertes.fr/hal-02305325`

[23] E. Sarrouy, Phase driven modal synthesis for forced response evaluation, in: 7 th International Conference on Nonlinear Vibrations, Localization and Energy Transfer, 2019.

[24] S. Bellizzi, R. Bouc, An amplitude-phase formulation for nonlinear modes and limit cycles through invariant manifolds, Journal of Sound and Vibration 300 (3-5) (2007) 896–915.

[25] T. Hill, S. Neild, A. Cammarano, An analytical approach for detecting isolated periodic solution branches in weakly nonlinear structures, Journal of Sound and Vibration 379 (2016) 150–165.

[26] Y. Sun, A. Vizzaccaro, J. Yuan, L. Salles, An extended energy balance method for resonance prediction in forced response of systems with non-conservative nonlinearities using damped nonlinear normal mode, Nonlinear Dynamics (2020) 1–19.

[27] M. Peeters, R. Viguié, G. Sérandour, G. Kerschen, J.-C. Golinval, Nonlinear normal modes, part ii: Toward a practical computation using numerical continuation techniques, Mechanical systems and signal processing 23 (1) (2009) 195–216.

[28] E. Petrov, A high-accuracy model reduction for analysis of nonlinear vibrations in structures with contact interfaces, Journal of Engineering for Gas Turbines and Power 133 (10) (2011) 102503.

[29] G. Battiato, C. Firrone, T. Berruti, B. Epureanu, Reduction and coupling of substructures via gram–schmidt interface modes, Computer Methods in Applied Mechanics and Engineering 336 (2018) 187–212.

[30] J. Yuan, F. Scarpa, G. Allegri, B. Titurus, S. Patsias, R. Rajasekaran, Efficient computational techniques for mistuning analysis of bladed discs: A review, Mechanical Systems and Signal Processing 87 (2017) 71–90.

[31] S. Rubin, Improved component-mode representation for structural dynamic analysis, AIAA journal 13 (8) (1975) 995–1006.

[32] R. Craig, M. Bampton, Coupling of substructures for dynamic analyses, AIAA journal 6 (7) (1968) 1313–1319.

[33] S. Zucca, B. I. Epureanu, Reduced order models for nonlinear dynamic analysis of structures with intermittent contacts, Journal of Vibration and Control 24 (12) (2018) 2591–2604.

[34] W. Witteveen, H. Irschik, Efficient mode based computational approach for jointed structures: joint interface modes, AIAA Journal 47 (1) (2009) 252–263.

[35] J. Yuan, L. Salles, C. Wong, S. Patsias, A novel penalty-based reduced order modelling method for dynamic analysis of joint structures, in: IUTAM Symposium on Model Order Reduction of Coupled Systems, Stuttgart, Germany, May 22-25, 2018.

[36] J. Yuan, L. Salles, F. El Haddad, C. Wong, An adaptive component mode synthesis method for dynamic analysis of jointed structure with contact friction interfaces, Computers & Structures 229 (2020) 106177.

[37] J. Yuan, C. Schwingshackl, C. Wong, L. Salles, On an improved adaptive reduced-order model for the computation of steady-state vibrations in large-scale non-conservative systems with friction joints, Nonlinear Dynamics (2020) 1–18.

[38] A. Fantetti, Tamatam, Volvert, Laval, Liu, L. Salles, M. Brake, C. Schwingshackl, D. Nowell, The impact of fretting wear on structural dynamics: experiment and simulation, Tribology International 138 (2019) 111–124.

[39] L. Salles, L. Blanc, F. Thouverez, A. M. Gouskov, P. Jean, Dynamic analysis of a bladed disk with friction and fretting-wear in blade attachments, in: ASME Turbo Expo 2009: Power for Land, Sea, and Air, American Society of Mechanical Engineers, 2009, pp. 465–476.

[40] E. Petrov, D. Ewins, Analytical formulation of friction interface elements for analysis of nonlinear multi-harmonic vibrations of bladed disks, Journal of turbomachinery 125 (2) (2003) 364–371.

[41] J. Yuan, A. Fantetti, E. Denimal, S. Bhatnagar, L. Pesaresi, C. Schwingshackl, L. Salles, Propagation of friction parameter uncertainties in the nonlinear dynamic response of turbine blades with underplatform dampers, Mechanical Systems and Signal Processing 156 (2021) 107673.

[42] Y. Sun, J. Yuan, E. Denimal, L. Salles, Nonlinear modal analysis of frictional ring damper for compressor blisk, Journal of Engineering for Gas Turbines and Power 143 (3) (2021) 031008.

[43] E. Sarrouy, J.-J. Sinou, Non-linear periodic and quasi-periodic vibrations in mechanical systems-on the use of the harmonic balance methods, in: Advances in Vibration Analysis Research, InTech, 2011.

[44] L. M. Amoo, On the design and structural analysis of jet engine fan blade structures, Progress in Aerospace Sciences 60 (2013) 1–11.

[45] E. Seinturier, Forced response computation for bladed disks industrial practices and advanced methods, Lecture Series-Von Karman Institute For Fluid Dynamics 2 (2007) 5.

[46] C. Joannin, B. Chouvion, F. Thouverez, M. Mbaye, J.-P. Ousty, Nonlinear modal analysis of mistuned periodic structures subjected to dry friction, Journal of Engineering for Gas Turbines and Power 138 (7).